# 3D Reconstruction of Specular Objects with Occlusion: A Shape-from-Scattering Approach

Yuki Hirofuji, Masaaki Iiyama, Takuya Funatomi, Michihiko Minoh

Kyoto University, Japan

**Abstract.** In this paper, we propose a method to measure specular objects regardless occlusion. The main contribution of this paper is that we have shown that the scattering of incident and specular reflection enable us to measure occluded surfaces. We locate objects in a tank filled with participating media, irradiate a laser beam to the objects, and observe the scattering of incident light and specular reflection. Occluded reflecting points of the laser are estimated from the peak pixel; scattering light that has local maximum intensity. Experimental results with a metallic specular plate demonstrate that our method can estimate the 3D position of occluded reflecting point.

## 1 Introduction

In a variety of fields, such as CG production and industrial design, it is important to measure the complete three-dimensional (3D) shape of objects. Most 3D shape measurement techniques acquire the shape of an object via reflected light from its surface; therefore, it is difficult to acquire specular objects, whose reflected light is highly directional and hard to observe with these techniques. While some techniques for measuring specular objects have been proposed, they cannot measure occluded surfaces.

In this paper we propose a new approach for measuring the shape of specular objects regardless of occlusion. In our approach, scattered light from a laser beam is used for the measurement. We place the object to be measured in a space filled with a participating medium, irradiate its surface with a laser beam, and observe the scattering in the participating medium as shown in Figure 1. As the laser beam passes through the medium, some of the light is scattered, and light reflected onto the surface is also partially scattered. In this situation, the path of the incident laser beam and the path of the specular reflection, which would not be observable in a clear air environment, can be observed as scattered light. Using this scattered light, we can estimate the location of the reflection points on the object's surface even when the surface is occluded.

## 2 Related Work

Most 3D shape measurement techniques such as stereo vision require the observation of reflected light from object surfaces. However, it is difficult to apply

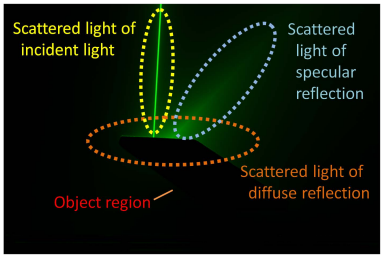


**Fig. 1.** The scenario for an object located in a tank filled with a participating medium

these techniques to measurement of specular objects because the reflected light from their surfaces changes greatly depending on the observing direction. Although several methods [1] for measuring specular objects have been proposed, including specular flow [2], the use of polarization [3], using a known pattern [4], and the shape-from-distortion method [5], none of these can be used to measure occluded shapes. The method proposed by Morris et al.[6] uses specular reflection for measuring shape of objects, and they considered scattering and refraction inside the object. Compared with this method, we assume scattering in participating medium and our method can measure occluded object shapes.

Velten et al. proposed a method that can measure occluded shapes [7]. This method is a time-of-flight (TOF) based measurement technique; that is, it measures the time required for laser light to be reflected off the object and returned to the detector. Their method requires the measured objects to be Lambertian objects; therefore it cannot be applied to measure specular objects. In addition, this method requires expensive femto lasers.

A study related to ours was performed by Hullin et al. [8]. They used fluorescent material for observing laser trails and succeeded in capturing transparent objects that are difficult to measure using most vision-based methods. In their method, scattering of laser trail is used for shape acquisition. However, this method does not consider a case wherein surface is occluded, and cannot also measure specular objects.

Recently, Iiyama et. al. proposed a method for acquiring occluded surfaces [9]. This low cost method uses the attenuation of reflected light to estimate the reflection points on occluded shapes; the attenuation is modeled by a $1/r^2$ law for a traveled distance $r$, and this model is fit to the observed image to estimate the location of the occluded reflection point. The drawback of this method is that it is not robust to image noise. The estimation is highly affected by this noise, because the low intensity pixels, which generally have a low S/N ratio, are necessary for the model fitting. In this paper, we extend this method so that it is robust to image noise. Instead of fitting a $1/r^2$ attenuation model, we use the locations of the scattered light peaks, that is, where a peak is a pixel that has a higher intensity than the pixels around it.

# 3 Measurement Using Reflection Peaks

## 3.1 Scattering

Our system configuration is shown in Figure 2. We placed an object into a tank filled with a participating medium in order to observe the scattered light of a laser beam. A laser unit mounted on a robot arm sent beams toward the object from the upper side of the tank. This robot arm was used for controlling the position of the laser beam.

The incident beams were scattered and were attenuated when they passed through the participating medium, and the beams were then reflected from the object surface. The reflected beams were also scattered and attenuated while passing through the participating medium. The light that was observed by the cameras was primarily comprised of the light scattered in the participating medium. As shown in Figure 1, the light scattered from the incident light was observed as a bright, bold, line-like region, the light scattered from the specular reflection appeared as a lobe shaped area, and that from the diffuse reflection appeared as a widely spread region. Even when the reflection point on the object's surface was occluded, this scattered light could still be observed.

We then estimate the location of the reflection point from this scattering from observed images. Our method uses at least two images taken from different viewpoints for estimating 3D location of single reflection point. It consists on (1) extraction of 2D candidate reflection points, (2) peak pixel detection for calculating the likelihoods, (3) identifying the candidate point with highest likelihood as 2D reflection point, and (4) 3D reflection point estimation.

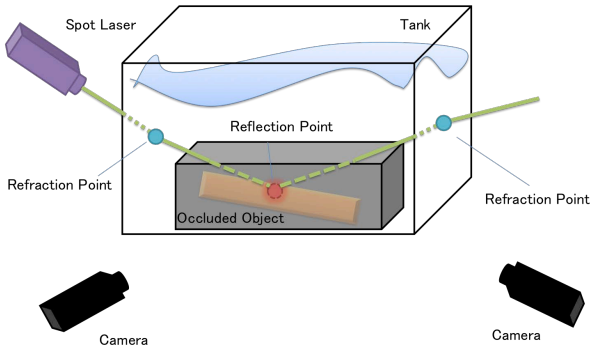


**Fig. 2.** Our system configuration: A robot arm with a spot laser was located on the upper side of the tank, and the spot laser was directed towards an object located within participating medium. The scattered light was observed with multiple cameras. Reflection point is occluded by other objects and can not be observed by the cameras.

### 3.2 Estimation of the reflection peaks

When we spot a laser on the object's surface and capture an image, its occluded reflection point on the image exists (1) along the line of the incident light on the images, and (2) in an object region obtained using a background subtraction method. The pixels that fulfill the two conditions are extracted and are designated pixels as "candidate points". Next, we calculate the likelihoods for each candidate point, and identify the candidate point with highest likelihood as the reflection point. The detailed methodology is presented in the following sections.

**Candidate points** To mask the object region, we employ a naive background subtraction method with pre-captured background and foreground images from the room under ambient light conditions. Although we can use more sophisticated methods, the masking in our method does not need to be highly accurate unless the masked region completely covers the entire object region. The remainder of this process will continue to work correctly even if some of the scattering region is contained by the masked region.

We extract the region that corresponded to the incident laser beam and extract the line of the incident light. As described in Section 3.1, the incident laser beam is observed as a bright, bold, line-like region, so we binarize the image with a constant threshold and extract the bold line-like region. We start from a high threshold and continuously lower it until the line-like region is extracted from Fig.3 as shown in Fig.4 Applying a Hough transform to the extracted region, the line of the incident light is detected. Note that since the extracted region has a rectangular shape, a diagonal of this rectangular region, which does not correspond to the line of the incident light, would also be detected. To avoid this, we apply a thinning operator before applying the Hough transform.

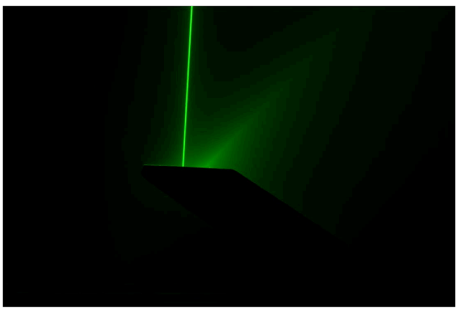

**Fig. 3.** An observed image. We can observe that the irradiated incident light from upper side is reflected to upper right in this image.

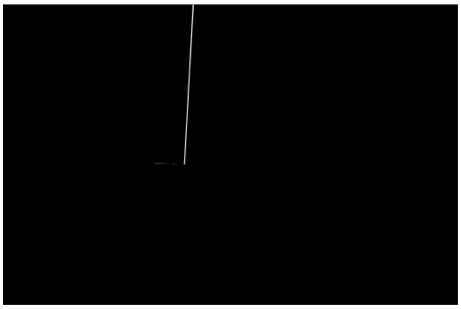

**Fig. 4.** The image of the extracted incident light from Fig.3.

Let $O$ be the object region and $S_I$ be the line of the incident light. The reflecting point exists on the line of the incident light and within the object region, thus a set of candidate points is defined by $C = S_I \cup O$. We use these candidate points in the following procedure.

**Extraction of peak pixels** A peak pixel is a pixel that has a higher intensity than the pixels around it, and it is defined as below. Let $\boldsymbol{r} = (r_x, r_y) \in \mathbb{R}^2$ be a pixel and $I(\boldsymbol{r}) \in \mathbb{R}$ be the intensity of a pixel $\boldsymbol{r}$ in an input image. For given a line $l = \{t\boldsymbol{d}(\phi) + \boldsymbol{r}_0\}$, an intensity profile along the line $l$ is given by

$$S_{\phi,\boldsymbol{r}_0}(t) = I\left(t\boldsymbol{d}(\phi) + \boldsymbol{r}_0\right) \tag{1}$$

where $t \in \mathbb{R}, \boldsymbol{d}(\phi)$ is the line direction $\boldsymbol{d}(\phi) = (\cos\phi, \sin\phi), 0 \leq \phi < 2\pi$, and $\boldsymbol{r}_0$ is a pixel position $\boldsymbol{r}_0 \in \mathbb{R}^2$. We define a peak pixel to be a pixel that has the local maximum intensity in the intensity profile. For all peaks $\boldsymbol{p}$, an angle $\phi$ and a positive value $\delta$ that satisfies the following condition exist.

$$S_{\phi,\boldsymbol{p}}(t) \leq S_{\phi,\boldsymbol{p}}(0)\ (-\delta \leq^{\forall} t \leq \delta), \tag{2}$$

The peak forms a roof edge at $t = 0$ on a line $l$. Fig.5 presents an example case in which one point on the line of the incident light is a peak of a profile $S_{\phi,\boldsymbol{r}_0}(t)$ .

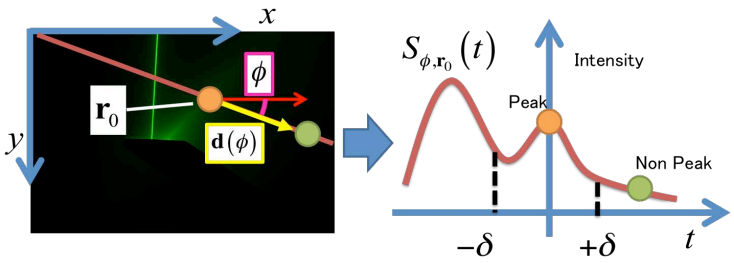


**Fig. 5.** A profile and the peak pixel. An orange-colored peak pixel on specular reflection has local maximum intensity in $S_{\phi,\boldsymbol{r}_0}(t)$, on the other hand, non peak pixel that is green-colored has NOT local maximum intensity in any direction $\phi$.

A reflection point is located on a line of specular reflection; that is, if the peaks are acquired correctly, they will be a strong clue for detection of the reflection points. We extract the peak pixels in regions of the obtained image excluding $O$.

Ideally, the profile will form a smooth curve and have peaks that are easy to extract, as illustrated the right panel of Fig.5, however, the profile will actually

contain noise. The accuracy of peak detection deteriorates due to the effect of noise and thus "fake" peaks may be extracted. However, the "true" peaks are still detected near the true position because the gradient of the intensity at the true (non-noise) peaks is sufficiently strong in the case where specular reflections exist.

We extract peak pixels along $x$-axis ($\phi = 0$) and $y$-axis ($\phi = \pi/2$) instead of a search for $\phi$. In the peak pixel extraction along $x$-axis, for all pixels $\boldsymbol{r}$ in an observed image, we compare $I(\boldsymbol{r})$ and intensity of all pixels around $\boldsymbol{r}$, $D = \{\boldsymbol{r}_t = (r_x + t, r_y)| - \delta \leq t \leq \delta, \delta > 0\}$ and test whether $\boldsymbol{r}$ satisfies the condition (2). Here, $\delta$ is constant through all peak pixel extraction. If $I(\boldsymbol{r})$ has maximum value among all $I(\boldsymbol{r}_t)$, the pixel $\boldsymbol{r}$ is extracted as a peak pixel. The same is true for $y$-axis. Even if direction of specular reflection is given by $\phi$ $(\phi \neq 0, \pi/2)$ as shown in Fig.5, pixels on the specular reflection will be extracted as peak pixels, when we only check with respect to $\phi = 0$ and $\pi/2$.

The fragility of the peak detection is also addressed in the likelihood calculation for the candidate points, as described below. We extract the peaks and express them as a binary image $P(\boldsymbol{r})$; the peak pixels are denoted by 1, and the other pixels by 0.

**Estimation of the reflection point locations** We estimate the location of the reflection point from $P(\boldsymbol{r})$, the observed image $I(\boldsymbol{r})$ and the candidate points $C$. In order to determine the reflection point from $C$, we focus on a half line $l_{\boldsymbol{c},\theta}$ which begins from a candidate point $\boldsymbol{c} \in C$ toward a direction $\theta$. Specular reflection exists on a line that passes through a reflection point, and specular reflection is extracted as peak pixels, thus if $\boldsymbol{c}$ is the reflection point, there must be a half line $l_{\boldsymbol{c},\theta}$ along which the peak pixels exist. Using this idea, we define a likelihood $L(\boldsymbol{c}, \theta)$, which is defined as the number of peak pixels weighted by the pixel intensities.

$$L(\boldsymbol{c}, \theta) = \int_0^{t_{\max}} P(\boldsymbol{r}) I(\boldsymbol{r}) dt \tag{3}$$

$$\boldsymbol{r}(t) = \boldsymbol{c} + t\boldsymbol{d} \tag{4}$$

$$\boldsymbol{d} = (\cos\theta, \sin\theta)\,, \tag{5}$$

where $t_{\max}$ is the distance from $\boldsymbol{c}$ to a border of the input image. By assigning a low weight to lower intensity peaks, which are sensitive to noise, we address the fragility of the peak detection. Note that peak pixels which corresponds to the incident light make a line, so we exclude the incident light region before the peak pixel extraction. The likelihood $L(\boldsymbol{c})$ of a possible reflection point is defined by using $L(\boldsymbol{c}, \theta)$ as

$$L(\boldsymbol{c}) = \max_{0 \leq \theta < 2\pi} \{L(\boldsymbol{c}, \theta)\}\,, \tag{6}$$

The point $\boldsymbol{c}$ which has the maximum $L(\boldsymbol{c})$ is estimated to be the reflection point $\boldsymbol{e}$. In short,

$$\boldsymbol{e} = \arg\max_{\boldsymbol{c} \in C} \{L(\boldsymbol{c})\}\,.$$

Fig.6 illustrates the procedure for calculating the likelihood $L(\boldsymbol{c}, \theta)$.

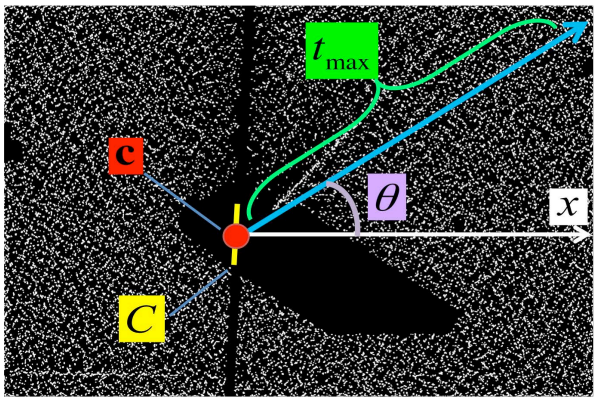


**Fig. 6.** Calculation of the likelihood

### 3.3 3D reflection point reconstruction

Generally, a point on a camera image corresponds to a 3D view line in the real world. However, due to refraction, in our experimental setup, it corresponds to a polyline; therefore, traditional computer-vision based stereo methods cannot be used for determining the reflection point position.

In our method, we reconstruct the 3D position of the reflection point from a single 2D reflection point on a camera image and two position on the line of the incident light of the other camera image. For each camera, we estimate the 2D reflection point, and select one camera $Cam_i$ which detect the 2D reflection point $\boldsymbol{e}$ with the highest likelihood $L(\boldsymbol{e})$. We calculate the 3D position of $\boldsymbol{e}$ as follows (see Fig.7).

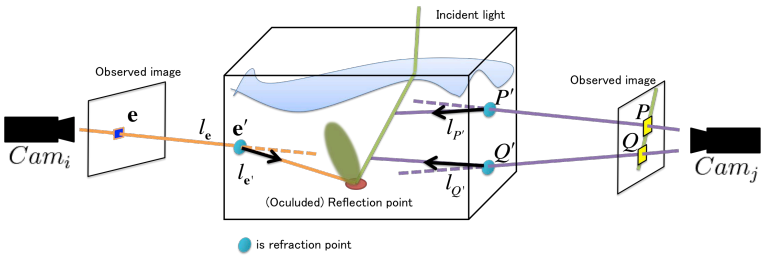


**Fig. 7.** We estimate a reflection point using camera B and calculated a plane $\pi$ using camera A; the reflection point is given by the 3D location of the intersection.

Let $\boldsymbol{e}$ be a 2D reflection point on $\mathrm{Cam}_i$ image, and $\boldsymbol{P}$ and $\boldsymbol{Q}$ be two position on the line of the incident light on $\mathrm{Cam}_j$ image. We first calculate $\boldsymbol{e}'$, $\boldsymbol{P}'$ and $\boldsymbol{Q}'$

which are refraction point of $\boldsymbol{e}, \boldsymbol{P}$ and $\boldsymbol{Q}$, and view line inside the tank $\boldsymbol{l}_{\boldsymbol{e}'}, \boldsymbol{l}_{\boldsymbol{P}'}$ and $\boldsymbol{l}_{\boldsymbol{Q}'}$. $\boldsymbol{l}_{\boldsymbol{e}'}, \boldsymbol{l}_{\boldsymbol{P}'}$ and $\boldsymbol{l}_{\boldsymbol{Q}'}$ satisfy,

1. Incident light exists on a plane whose normal vector is $\boldsymbol{l}_{\boldsymbol{P}'} \times \boldsymbol{l}_{\boldsymbol{Q}'}$ and that includes $\boldsymbol{l}_{\boldsymbol{P}'}$ and $\boldsymbol{l}_{\boldsymbol{Q}'}$ in 3D space.
2. A reflection point exists on a line $\boldsymbol{l}_{\boldsymbol{e}'}$.

From 1. and 2., the 3D position of reflection point is obtained as intersection of the plane in 1. and the line in 2.

We obtain the 3D shape of objects by applying the above procedure while changing the position of the laser beam.

## 4 Experiments

To create a participating medium, about 180 L of water and 1 mL of milk are mixed in a 60 cm cubic tank, and were filtered in order to eliminate dust in the tank. According to Narashimhan et al.[10], in the case where 24 L of water and 15 mL of milk are mixed, the scattering coefficient $\sigma_s$ is $1.3293 \times 10^{-2}$ $[mm^{-1}]$. As the scattering coefficient is proportional to density, it is $\sigma_s = 1.1324 \times 10^{-4}$ $[mm^{-1}]$ in our experimental environment; thus, multiple scattering light could be ignored because second scattering coefficient is $\sigma^2$. We used four cameras, two of which were placed on one side of the tank and the other two of which were orthogonally located on the other side of the tank as shown in Figure 8. The cameras were Nikon D7000 single lens reflex cameras, with $4948 \times 3280$ pixels.

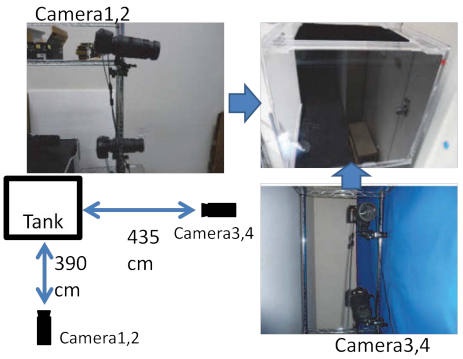


**Fig. 8.** Locations of the cameras and the tank.

### 4.1 2D reflection point estimation

We compared the accuracy of the 2D reflection point estimation from our method with that derived using Iiyama et. al. 's attenuation-based method. Note that,

since it can be difficult to determine ground truth reflection points, we used a metallic plate to facilitate their acquisition (Fig. 9).

In order to determine the ground truth, we used a non-occluded scene for the evaluation as shown in Fig.10. Masking the object region, we simulated an occluded scene (Fig.12), and used images that is removed peak pixels on incident light and around object region for further experiments (Fig. 13). We used nine reflection points on the metallic plate. Table 1 lists the errors (in pixels) in the estimated point locations with respect the correct point locations for the attenuation-based method and our new method. Each error value is averaged over the nine points. In our setup, one pixel is generally equivalent to 0.3 mm.

**Table 1.** Average errors for the attenuation-based method and our new method (in pixels).

| Estimation | cam1 | cam2 | cam3 | cam4 |
|---|---|---|---|---|
| attenuation-based method | 76.4 | 147.6 | 275.4 | 350.8 |
| proposed method | 11.8 | 27.3 | 71.6 | 62.6 |

The average error of our method is about 1/10 obtained when using the attenuation-based method. Fig. 14 shows the peak image and detected reflection point with respect to the image shown in Fig. 13. This result demonstrates that our method can measure specular surfaces even if they are occluded.

**Fig. 9.** A metalic plate used in 2D reflection point estimation.

### 4.2 3D reflection points estimation

In order to show that our method is able to perform 3D reconstructions, we measured the surface of the mirror shown in Fig 15. In this experiment, as with

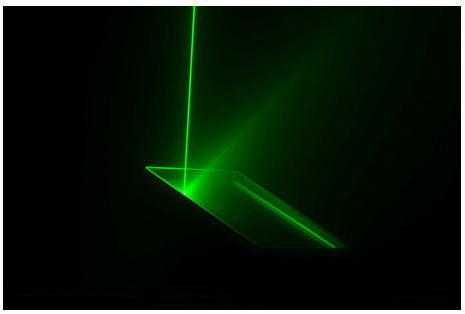

**Fig. 10.** An observed image.

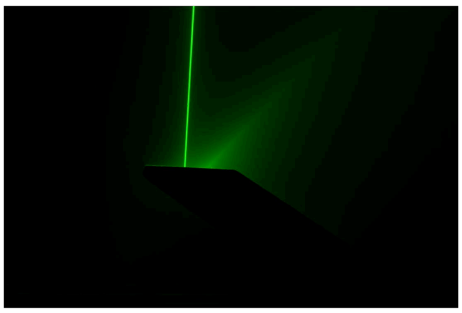

**Fig. 11.** A masked image by object region $O$. This image is obtained by Fig.10. We treat this image as an input image.

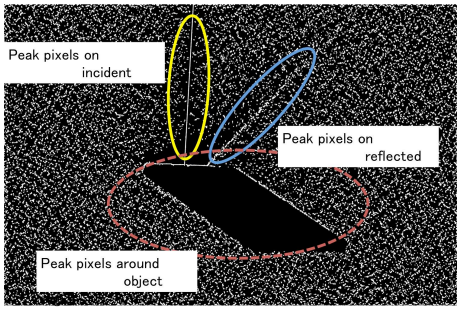


**Fig. 12.** A binary image extracted peak pixels from Fig.11. However, this image includes peak pixels on incident light and around object region.

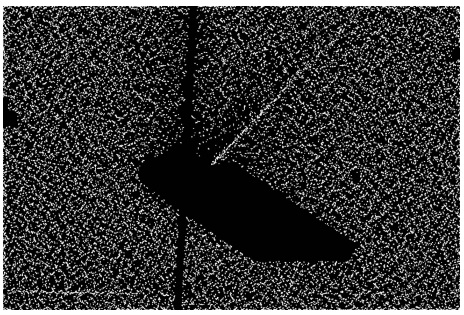

**Fig. 13.** A final image before performing the weighted Hough transform. Peak pixels on incident light and around object region is removed.

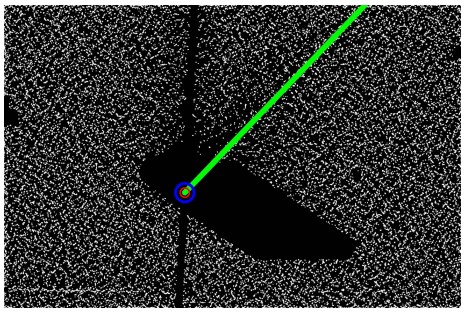

**Fig. 14.** An estimation result from Fig.13. A green line shows the direction has highest value in all $L(\boldsymbol{c}, \theta)$, and the center of circles shows the candidate point $\boldsymbol{c}$.

the experiment to evaluate the accuracy of our method, we masked the object region and measured pseudo-occluded shapes. The result of the reconstruction, comprised of about 100 reflection points, is shown in Fig. 16. Most the points exist on the same plane; that is, they have been correctly reconstructed.

An estimation failure, which can be observed at the edge of the mirror, was caused by the presence of multiple reflected lights with high intensities. A limitation of our method is that it works under the assumption of existence of specular reflection. In more detail, it cannot correctly measure a shape when multiple reflections are occurring.

A typical failure is shown in Fig. 18, which is the result produced for the ashtray shown in Fig. 17. Fig. 18 illustrates a scene in which light was incident from above, reflected to the left side of the ashtray surface, and then reflected at the tank many times (outside of the image shown). In this case, multiple reflection occurred inside and outside of the object region, we cannot estimate reflection points in principle under the scene. To find a solution of such multiple reflection is one aspect of our future work.

**Fig. 15.** A measured object, mirror used in 3D reflection points estimation.

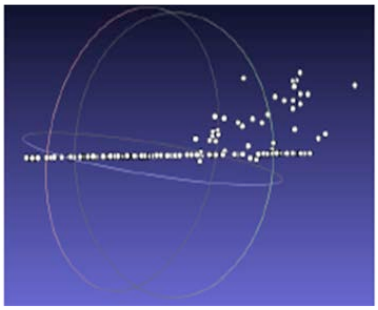

**Fig. 16.** Reconstruction result of the mirror. This image shows the result from the side. Many points exists on the same plane.

## 5 Conclusion

In this paper, we proposed a method that estimates the reflection points of specular objects regardless of occlusion. The peak pixels that have the highest local intensity in the scattered light were used for the estimation. Although the peak pixels are robust to image noise, we enhance their robustness against image noise by applying a weighted Hough transform.

Our method only works when specular reflection is clearly observed. In the case where specular reflection is not observed, this method will instead produce

**Fig. 17.** An ashtray used in 3D reflection points estimation.

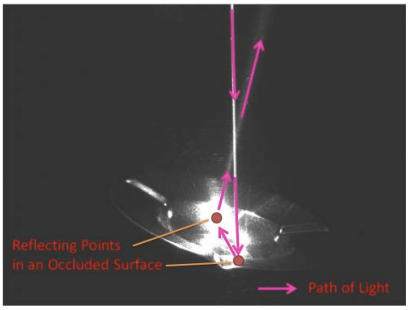


**Fig. 18.** Multiple reflection.

points that are significantly offset from the ground truth. Despite this drawback, our method presents a significant contribution that scattering of specular reflection can provide valuable clues for measuring occluded surfaces.

Improvement of the peak detection is one task planned for our future research. In addition, in our implementation it takes around six minutes to process per one point estimation though we don't parallelize so we must improve processing time. This proposed method and our attenuation-based method could complement each other, and in a future work we will integrate these methods.

**Acknowledgement**. This work was supported by JSPS KAKENHI Grant Number 26700013.

## References

1. Ihrke I., Kutulakos K. N., Lensch H., Magnor M., and Heidrich W. "State of the art in transparent and specular object reconstruction," EUROGRAPHICS 2008 STAR-State of the Art Report, 2008, pp. 87-108.
2. Roth S., and Black M. J. "Specular flow and the recovery of surface structure," Proceedings of IEEE Conference on Computer Vision and Pattern Recognition (CVPR) (New York, NY, USA, 2006), pp. 1869-1876.
3. Clark J., Trucco E. and Wolff L. B. "Using light polarization in laser scanning," Image and Vision Computing 15, 1 (1997), pp. 107-117.
4. Kutulakos K. N. and Steger E. "A theory of refractive and specular 3D shape by light-path triangulation," In Proceedings of IEEE International Conference on Computer Vision (ICCV) (Beijing, China, 2005), pp. 1448-1455.
5. Schultz H. "Retrieving shape information from multiple images of a specular surface," IEEE Transactions on Pattern Analysis and Machine Intelligence (PAMI) 16, 2 (1994), 195-201.
6. Morris, Nigel JW, and Kiriakos N. Kutulakos. "Reconstructing the surface of inhomogeneous transparent scenes by scatter-trace photography." Computer Vision, 2007. ICCV 2007. IEEE 11th International Conference on. IEEE, 2007.

7. Velten A., Willwacher T., Gupta O., Veeraraghavan A., Bawendi M. G., and Raskar R. "Recovering three-dimensional shape around a corner using ultrafast time-of-flight imaging," Nature Communications (2012),3,745.
8. M.B. Hullin, M. Fuchs, I. Ihrke, H.-P. Seidel, and H.P.A. Lensch, "Fluorescent immersion range scanning," in Acm Transactions on Graphics, vol. 27, Issue 3, Article 87. Univ British Columbia, Vancouver, BCV5Z IM9, Canada, 2008.
9. Masaaki Iiyama, Shohei Miki, Takuya Funatomi, and Michihiko Minoh "3D Acquisition of Occluded Surfaces from Scattering in Participating Media," International Conference on Pattern Recognition 2014, 2014.
10. Narasimhan S. G., Gupta M., Donner C., Ramamoorthi R., Nayar S. K. and Jensen H. W. "Acquiring scattering properties of participating media by dilution," ACM Trans. Graph, Vol. 25, No. 3, pp. 1003- 1012 (2006).